



Research article

Assessing the long term effects on climate change of metallurgical slags valorization as construction material: a comparison between static and dynamic global warming impacts

Andrea Di Maria^{1,*}, Annie Levasseur² and Karel Van Acker^{1,3}

¹ Department of Materials Engineering, Katholieke Universiteit Leuven (KU Leuven), Kasteelpark Arenberg 44 box 2450, BE-3001 Leuven, Belgium

² Department of Construction Engineering, École de technologie supérieure, 1100, Rue Notre-Dame Ouest, Montréal (Québec), H3C 1K3, Canada

³ Center for Economics and Corporate Sustainability (CEDON), KU Leuven, Warmoesberg 26, BE-1000 Brussels, Belgium

* **Correspondence:** Email: andrea.dimaria@kuleuven.be.

Abstract: The interest in circular economy for the construction sector is constantly increasing, and Global Warming Potential (GWP) is often used to assess the carbon footprint of buildings and building materials. However, GWP presents some methodological challenges when assessing the environmental impacts of construction materials. Due to the long life of construction materials, GWP calculation should take into consideration also time-related aspects. However, in the current GWP, any temporal information is lost, making traditional static GWP better suited for retrospective assessment rather than forecasting purposes. Building on this need, this study uses a time-dependent GWP to assess the carbon footprint of two newly developed construction materials, produced through the recycling of industrial residues (stainless steel slag and industrial goethite). The results for both materials are further compared with the results of traditional ordinary Portland cement (OPC) based concrete, presenting similar characteristics. The results of the dynamic GWP (D_GWP) are also compared to the results of traditional static GWP (S_GWP), to see how the methodological development of D_GWP may influence the final environmental evaluation for construction materials. The results show the criticality of the recycling processes, especially in the case of goethite valorization. The analysis shows also that, although the D_GWP did not result in a shift in the ranking between the three materials compared with S_GWP, it provides a clearer picture of emission flows and their effect on climate change over time.

Keywords: dynamic global warming potential; metallurgical slags valorization

1. Introduction

The construction sector accounts for one-third of the global greenhouse gas emissions, as well as for 50% of the globally extracted materials and 42% of the total European Union (EU) final energy consumption [1,2]. From these figures, the key role played by the construction sector in the quest for sustainability and the circular economy appears clear. In the past, the development of sustainability strategies for the construction sector has focused mainly on the energy demand of buildings during the use phase. Most recently, along with the increasing development of technologies for low-energy buildings, the attention of researchers has been drawn also to reducing the environmental burdens arising from the extraction of raw materials and the manufacturing of construction materials [2]. In the last decades, indeed, many fortunate stories have been told on successful implementations of material circularity in the construction sector, as well as on valorization of residues from other industrial sectors for the production of secondary construction materials. In this context, one of the best-known examples is the valorization of metallurgical slags as a substitute for cementitious binders in concrete and brick production. Although the technical feasibility of metallurgic slags valorization as cementitious material has been widely demonstrated (see, among others, Pontikes and Snellings (2014), Panesar (2019) [3,4]), environmental consequences are not yet entirely understood. Metallurgic slags can completely (or partially) replace ordinary Portland cement (OPC), whose manufacturing is an extremely energy-intensive process, responsible for 7% of global anthropogenic carbon dioxide emissions [4]. Considering that OPC alone represents 76% of concrete carbon emissions [5], the substitution of OPC could represent a key factor for the sustainability of concrete. On the other hand, slags may need several pretreatment steps before becoming suitable to be used as cementitious materials. Therefore, pretreatment processes such as drying, grinding, or transportation may offset the environmental benefits of OPC replacement.

Robust and comprehensive environmental assessment methodologies are therefore fundamental to fully understand potential environmental consequences from replacing primary with secondary materials. Global warming potential (GWP) is currently the most used indicator to account for carbon emissions and climate change effects of human activities. As defined by the Intergovernmental Panel on Climate Change (IPCC) (see for instance Myhre (2013) [6]), GWP assesses and compares the effect of greenhouse gases in the atmosphere, measuring radiative forcing caused by the emission of a unit of greenhouse gas over a specific time, defined as time horizon [6]. Although GWP values are very sensitive to the chosen time horizon, GWP is typically used to assess life cycle GHG emissions as a single aggregated emission, losing all temporal information. The loss of temporal information is considered as one of the most important factors that decrease the accuracy of global warming impact assessments [7–11]. Indeed, releasing a large quantity of pollutants instantaneously generally does not have the same impact as releasing the same quantity of pollutants at a small rate over several years [12].

Accounting for the timing of greenhouse gas emissions and uptakes is relevant for the carbon footprint of construction materials because it allows considering the impact of temporarily storing carbon or delaying GHG emissions along the lifetime of buildings [13]. Carbon uptake by

construction materials is indeed one of the most important phenomena affecting the sustainability of materials such as concrete or wood [14]. Many authors have previously investigated the effects of including temporal information when assessing the environmental impacts of buildings. Among others, some of these authors focused on the importance of dynamic inventories [15–18], while other authors focused specifically on the assessment of dynamic GWP for buildings [19,20] and construction materials [21]. For instance, Negishi [18] developed a method for dynamic inventory for both background and foreground processes, using the temporal distribution archetypes for ecoinvent 3.2 as described by Tiruta-Barna [22]. Mastrucci [20] enlarged temporal aspects to both inventory and impact assessment phases, respectively considering the evolution of housing stocks (for dynamic inventory) and applying time-adjusted carbon footprint calculation (for dynamic impact assessment). Resch [19] proposed a novel method for estimating the long-term impacts on climate change due to material used in buildings, by creating a dynamic inventory and then including the temporal dimension in the calculation of the climate change effects. Fouquet [23] combined a perspective life cycle inventory with a dynamic GWP assessment for carbon emissions, investigating how the temporal aspects affect the results for three single houses built with different construction materials. A certainly more exhaustive review on dynamic assessment applied to buildings can be found in Su and Beloin Saint-Pierre [24,25]. From the analysis of previous literature, we can conclude that considering temporal information when assessing global warming impacts allowed to consistently consider the timing of emissions. Results showed how the application of a dynamic approach for global warming impacts allows for a more informed analysis of emissions flows and climate change effects over time. To the knowledge of the authors, the study by Fouquet is the only available study in the literature focusing on dynamic GWP of construction materials. Also, there is no study available today on dynamic GWP applied to recycled materials.

Building on this need, this work focuses on the comparison of static and dynamic global warming impacts for two case studies in which metallurgical slags substitute OPC-based concrete as construction blocks for building insulation. The first case presents the valorization of slags from stainless steel production, while the second case study presents the use of goethite slags from zinc production. Results for both cases studies are compared using static and dynamic GWP for traditional OPC-based insulation concrete presenting similar characteristics.

2. Methods and materials

Section 2 presents some general information on the differences between static and dynamic GWP and on the valorization of goethite and stainless steel slags (SSS).

2.1. Static and dynamic global warming potential (GWP)

The calculation of the GWP is based on the calculation of the emission radiative forcing, which represents the net change in the energy balance of the atmospheric earth system due to the emission of a specific gas, and it is expressed in Watts/m² averaged over a particular time [6]. The GWP, as expressed by the IPCC AR5 [26], is the cumulative radiative forcing caused by the emission of a unit mass of given greenhouse gas over a defined time horizon, normalized to the equivalent radiative forcing of CO₂. The GWP definition from IPCC can be expressed mathematically through Eq (1) [12]:

$$GWP_i^{TH} = \frac{AGWP_i^{TH}}{AGWP_{CO_2}^{TH}} = \frac{\int_0^{TH} a_i[C_i(t)dt]}{\int_0^{TH} a_{CO_2}[C_{CO_2}(t)dt]} \quad (1)$$

where GWP_i^{TH} is the static GWP for an emitted gas i calculated for a time horizon TH , $AGWP_i^{TH}$ and $AGWP_{CO_2}^{TH}$ represent the cumulative radiative forcing for gases i and CO_2 respectively (also called absolute GWP) over the same time horizon TH , a_i and a_{CO_2} are the instantaneous radiative forcing per unit mass increase, C_i and C_{CO_2} are the time-dependent atmospheric load of the gases. The atmospheric load following a pulse emission $C(t)$ for carbon dioxide is given by the Bern carbon cycle-climate model, while $C(t)$ for other greenhouse gases is given by a first-order decay equation [6]. GWP is thus a normalized metric since it converts the cumulative radiative forcing for a generic gas i into the CO_2 equivalent radiative forcing.

The first IPCC Assessment Report proposed three different time horizons for GWP calculation: 20, 100, and 500 years. The 100-year time horizon is mostly used because of its adoption for the application of the Kyoto Protocol, but it is not scientifically more relevant or justified compared to any other time horizon [27]. Nonetheless, the choice of a time horizon significantly affects the value of GWP for short-lived gases such as methane. As shown in Figure 1, cumulative radiative forcing for methane reaches its maximum over the first years following the emission, while for CO_2 , it increases constantly over time. Therefore, since GWP_{CH_4} is the relative effect $AGWP_{CH_4}/AGWP_{CO_2}$, GWP for methane decreases with increasing time horizons, as the numerator remains constant after the peak, while the denominator $AGWP_{CO_2}$ continues to rise over time [28].

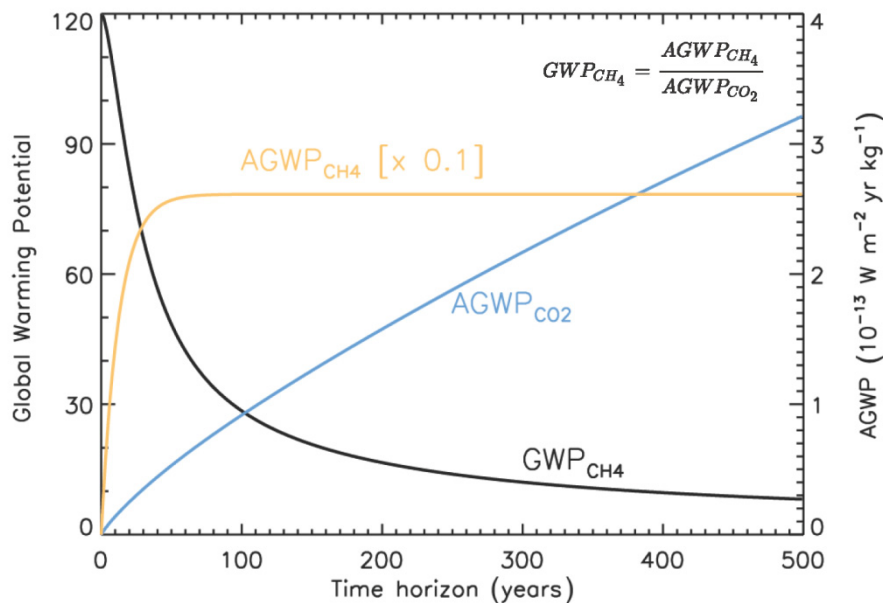


Figure 1. Time-dependent variation of cumulative radiative forcing (AGWP) for a pulse emission of methane and CO_2 (source IPCC (2013) [28]).

The use of traditional GWP with fixed time horizons has been debated in the last decades, as it may present inconsistencies between the time horizon chosen for the analysis and the actual time covered by the results [12]. To overcome these inconsistencies, characterisation factors with flexible time horizons have been developed recently, and they have been used for the calculation of a time-dependent GWP (the dynamic GWP), to correctly represent the effect of timing of the

emissions. The dynamic GWP model, as it is developed by Levasseur [12], calculates two time-dependent parameters: the *Instantaneous Global Warming Impact* $GWI(t)_{\text{instantaneous}}$ and the *Cumulative Global Warming Impact* $GWI(t)_{\text{cumulative}}$. These parameters are based on the development of dynamic characterization factors (DCFs), which are calculated integrating $AGWP_i$ continuously over time. $DCF_i(t)_{\text{cumulative}}$ obtained with Eq (2) represents the cumulative radiative forcing per unit mass of GHG released into the atmosphere since the emission occurred.

$$DCF_i(t)_{\text{cumulative}} = AGWP_i \int_0^t a_i \cdot [C_i(t)] dt \quad (2)$$

To obtain the instantaneous value $DCF_i(t)_{\text{instantaneous}}$ for any year following the emission, the time-scale is divided into one-year time steps, and the integration boundaries must be set for every time-step:

$$DCF_i(t)_{\text{instantaneous}} = \int_{t-1}^t a_i \cdot [C_i(t)] dt \quad (3)$$

Finally, to calculate the time-dependent global warming impacts GWIs for the considered life cycle, the DCFs must be combined with the dynamic inventory. The dynamic inventory for each GHG is built by dividing the analyzed life cycle by one-year time steps, and adding the different emissions for each GHG, for every time-step:

$$GWI(t)_{\text{instantaneous}} = \sum_i GWI_i(t) = \sum_i \sum_{j=0}^t [(g_i)_j \cdot [DCF_i]_{t-j}] \quad (4)$$

where $(g_i)_j$ represents the inventory result of any gas i at time j , and DCF is the instantaneous characterization factor for any gas i at time j .

Finally, Eq (5) calculates the cumulative $GWI_{\text{cumulative}}$ ($W \cdot yr \cdot m^{-2}$) as the sum of the $GWI_{\text{instantaneous}}$ calculated for all the years from zero to t .

$$GWI(t)_{\text{cumulative}}(t) = \sum_{i=0}^t GWI_{\text{inst}}(t) \quad (5)$$

The current paper investigates the differences between static and dynamic GWP results. The dynamic GWP is calculated using the software DYNCO2, which contains the DCFs calculated for all GHGs. By feeding the model with the exact emissions per GHG per year, DYNCO2 calculates the evolution of the global warming impact over time, using the equations described above.

2.2. Construction materials from goethite

Goethite ($\alpha\text{-FeOOH}$) is one of the main constituents of the iron oxide residues in zinc hydrometallurgy. Goethite is formed to remove iron from the zinc solution, as iron constitutes a severe impurity and must be precipitated before zinc electrolysis [29,30]. Goethite presents 5–10% content in zinc, as well as traces of other valuable metals. This concentration of zinc is too high to enable goethite recycling in iron production and, on the other hand, too low to make zinc recovery economically profitable [31]. Therefore, impoundment in controlled tailings ponds is today one of the most common end-of-life treatments for goethite. The impoundment of goethite represents today

a high economic cost for the hydrometallurgical industry, and it constitutes also a potential environmental hazard for society, due to the risk of leaching of heavy metals and hazardous elements [29–32].

In recent years, many scientific researchers have focused on the potential recovery of valuable metals from goethite [33–39]. Among others, one of the most promising goethite valorization processes is the combination of plasma fuming and subsequent inorganic polymerization of the fumed fraction residues. In plasma fuming, goethite can be heated by electric torches to vaporize metals, that are later precipitated and recovered in the form of metals oxides [40–43]. Recovered metal oxides can be used by metal smelters in secondary metals production, replacing the need for metal concentrates from primary ores. Left-overs of the plasma fuming, the fumed fraction, is a metal-free slag that can be further valorized by mixing with an alkaline-silicate activator, to produce a high strength inorganic polymer with a non-carbon-based skeletal structure [44,45]. This produced inorganic polymer can be used as a construction material, replacing traditional cement-based concrete.

2.3. Construction materials from stainless steel slag

Stainless steel slag (SSS) is a residue occurring during the production of stainless steel, composed mostly of calcium and silica oxides. SSS presents several properties that could allow further valorization as secondary raw material. For instance, SSS could represent a feed source for secondary chromium, nickel and iron [46]. Moreover, SSS presents pozzolanic properties that make it suitable for potential valorization as raw material for road construction or cement production [47]. Despite these opportunities, the valorization rate of SSS is currently rather limited [48]. One of the main reasons hindering SSS valorization is its tendency to disintegrate into fine dust, which makes slag handling problematic and also causes the loss of some technical properties, making SSS not suitable to be used as a hydraulically active additive in the cement industry [49]. On top of that, the heavy metal content of SSS, especially chromium, restricts the SSS valorization in many other applications [49,50]. It is well established today that SSS disintegration phenomena can be avoided by adding borates during the cooling phase, in a quantity equal to 2% of the total mass of the SSS [51]. The SSS stabilized with borates can also be recycled as low-quality aggregates to be used as filling materials for embankments and road construction.

However, stabilization through borates addition and valorization as filling material can be considered as a low-value application for the high-quality oxides contained in the SSS [52]. Therefore, recent research has investigated the possibility of recycling SSS as a secondary binder for new construction materials, replacing traditional OPC [53–55]. In this framework, one of the most promising routes is the activation of SSS through the alkali activation process. As described by Provis [56], an alkali activated material is a binder system derived from the reaction of an alkali source (e.g. silicates or carbonates) and a solid silicate powder (e.g. metallurgic slag). If sand and gravel are also added in the alkali activation process, the activated SSS acts as a binder to form a high-strength and high-stable block that can be used as construction block, replacing traditional OPC-based concrete.

3. Global warming impact assessment of construction materials

Section 3 presents the calculation of static and dynamic global warming impact for the two construction materials from goethite and SSS valorization. First, the goal, functional unit and system boundaries of the study are presented. Secondly, the inventory section presents the technical process for valorizing the slags and data collection. Finally, the impact assessment section details the static and dynamic GWP calculations and presents the global warming impact for the construction blocks using both approaches.

3.1. Goal, scope, and functional unit

The goal of the study is to assess the life cycle global warming impact of three different insulation construction materials: (i) traditional autoclaved aerated OPC concrete (OPC_{aer}); (ii) goethite-based inorganic polymers (GIP); (iii) stainless steel slag-based alkali activated aerated blocks (SSS_{aer}).

The study performs two separate global warming impact calculations based on different measures: a traditional static GWP (S_GWP), and a dynamic GWP (D_GWP). The comparison of the results from the two approaches can help to understand the advantages of using a dynamic approach in the calculation of the global warming long-term effects, especially when analysing products with long life cycles.

The functional unit is the reference to which all inputs and outputs of the study refer, and it must ensure a fair comparison among the products. The functional unit adopted for this study is the insulation capacity of one m^2 surface for the three different insulation materials, all produced in Belgium. Table 1 shows that the thermal conductivity of GIP is higher than the one of OPC_{aer} and SSS_{aer} . Since all materials must ensure the same insulation capacity, the thickness of the considered GIP block must be higher than the one of OPC_{aer} and SSS_{aer} . Therefore, assuming a thickness of 5 cm for OPC_{aer} and SSS_{aer} , the required thickness for GIP block is 6 cm.

3.2. Temporal and physical system boundaries

This study considers the whole life cycle of materials. Pommer [57] suggested using a time frame of 100 years, including the use phase and EOL/secondary life of concrete, although the lifetime depends on the quality of the material and the ageing conditions of the building. This study assumes 50 years as an average lifetime for all the considered materials, composed of three phases: production (at year 1), use-phase (from year 1 to year 50), end-of-life (from year 50 to year 100). Table 2 shortly describes the various temporal phases of the life cycles for the three materials, while Figure 2 defines system boundaries including the whole life cycle of the three materials (cradle to grave). The following paragraphs detail the production, use, and end-of-life phases for each material.

Table 1. Main physical properties and reference quantities for each of the three materials. All quantities refer to the reference flow of 1 m².

	Autoclaved aerated OPC concrete (OPC _{aer})	Goethite-based inorganic polymers (GIP)	Alkali-activated aerated SSS blocks (SSS _{aer})
Materials properties			
Thermal conductivity [W·(m·K) ⁻¹]	0.15	0.18	0.15
Compressive strength (MPa/m ²)	4.1	4.6	10
Density (g/cm ³)	0.6	1.04	1.16
Dimensions of 1 block (cm)	10×20×5	10×20×6	10×20×5
Reference flow (1 m²)			
Blocks (n°)	50	50	50
Volume (m ³)	0.05	0.06	0.05
Weight (kg)	30	62.4	58

Table 2. Lifetime frames for the three materials.

Year	Life cycle phase	Description
1	Production	Materials are produced.
1–50	Use phase	Materials are placed in buildings. During this phase, a carbonation process (CO ₂ uptake) occurs.
50–100	End-of-life	Materials are recycled as aggregates (90%) or landfilled (10%). Carbonation process still occurs in this phase.

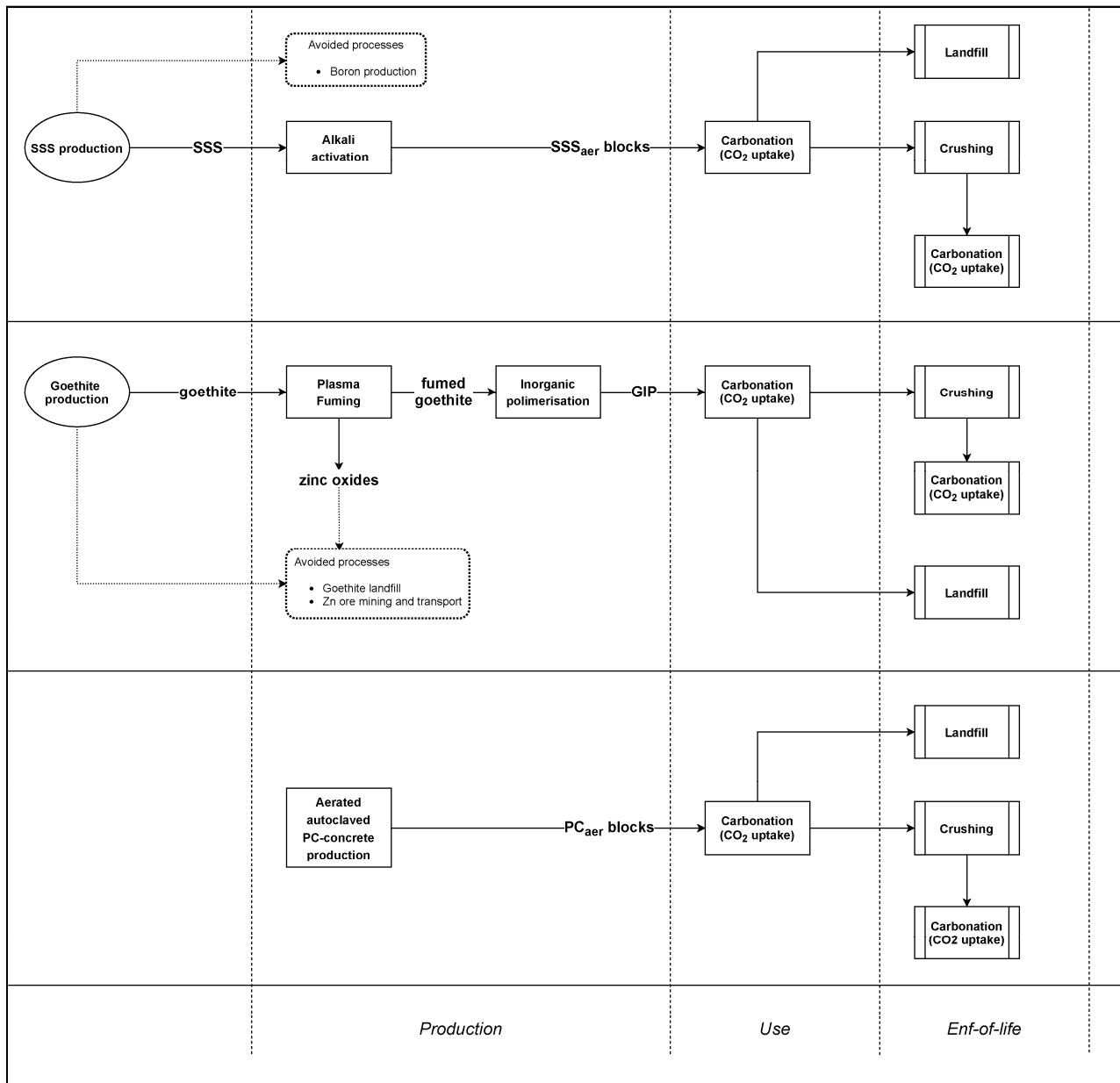


Figure 2. System boundaries considered in the study.

3.3. Inventory data

3.3.1. Production phase

SSS_{aer} is made through alkali activation, using SSS as a precursor. SSS_{aer} is a lightweight aerated material with a porous internal structure. Porosity increases the insulation (thermal and acoustic) capacity of SSS_{aer} . A 0.4 wt% of aluminum powder is added to the mix during the alkali activation process to obtain this porous internal structure. Aluminum aids the foaming process creating small air bubbles that are trapped into the structure of the block, creating the porous structure. Transport distances can significantly vary from case to case, therefore some assumptions are required. Availability of primary resources to produce construction materials is usually limited, and these resources are frequently transported from remote areas, while secondary resources for

construction materials are mostly utilized in the proximity of the production sites [58,59]. Therefore, the use of secondary construction raw materials leads to a transport distance reduction compared to the use of primary construction materials. Based on previous studies on concrete and slags from stainless steel processes (see for instance Martaud and Mroueh [60,61]), this study assumes 10 km distance from the stainless-steel plant to the production factory, where the SSS_{aer} is produced, while avoided transport of the stabilized stainless-steel slag to the low-quality aggregate application is assumed to be 50 km. All inventory data for SSS_{aer} refers to the studies from Di Maria and Salman [53,54].

GIP block is made from goethite that is plasma fumed in Norway. Subsequently, fumed residues and metal oxide powder are collected and shipped 1,500 km from Norway to Belgium. Fumed residues go through the inorganic polymerization process to produce inorganic polymer for insulation purposes. Metal oxides powder is sold to the local smelters for the production of secondary zinc. The inventory data for GIP block production refers to the study of Di Maria [31].

Finally, the OPC_{aer} production phase refers to the design mix of cement, gravel, sand and water, which is needed to provide concrete performances such as compressive strength and durability. The OPC-concrete mix to provide required thermal conductivity and compressive strength is calculated using the BRMCA methods from the British Ready Mix Design Association [62].

All inventory data used for GIP, SSS_{aer} and OPC_{aer} production are summarized in Table 6 in the supplementary materials.

3.3.2. Use phase

The use phase of the three materials is assumed to be 50 years, during which CO_2 uptake will occur. CO_2 uptake for OPC_{aer} is calculated by using the mathematical model presented in Pommer and Pade (2006) [57]. Concerning CO_2 uptake for GIP and SSS_{aer} , no mathematical model is currently available, and several assumptions based on a literature review had to be made as described in the following paragraphs.

3.3.2.1. Carbonation rate for the autoclaved aerated OPC-based concrete

Carbonation in the atmospheric environment has been extensively studied during the lifetime of concrete structures, and mathematical models are available to calculate the carbonation rate of OPC-based concrete over time [63–65].

Carbonation rate depends on various elements: the volume of material exposed to the atmosphere, the strength class, and the type of binder. The amount of CO_2 that can be absorbed by a given volume of a specific material is calculated with Eq (6):

$$CO_{2_uptake} [kg] = CaO_{available} [\%] \cdot Cement_{concr} \left[\frac{kg_{cement}}{m^3_{concrete}} \right] \cdot Clinker_{cement} [\%] \cdot CaO_{clinker} [\%] \cdot \text{mole fraction} \left[\frac{gCO_2/molCO_2}{gCaO/molCaO} \right] \cdot V_{carb} [m^3] \quad (6)$$

where CO_{2_uptake} represents the amount of CO_2 that can be absorbed by the given volume V_{carb} . The values of the different parameters used to calculate the CO_{2_uptake} are reported in Table 3. Considering that all available volume of material can be carbonated ($0.05 m^3$, as shown in Table 1), the amount of CO_2 uptaken by OPC_{aer} is equal to 2.61 kg.

Table 3. Values of constant (in time) parameters to calculate CO₂ uptaking.

Parameter	Value	note	Reference
CaO _{available}	75%	Calcium oxide in cement that is available for carbonation	[64]
Cement _{concr}	144 kg/m ³	Kg of Cement content in 1 m ³ of concrete	Calculated from inventory data
Clinker _{cement}	95%	Content of clinker in cement	[66]
CaO _{clinker}	65%	CaO content in clinker (assumption)	[57]
Mole fraction	0,78	Molecular mass CO ₂ / molecular mass CaO	Calculated
V _{carb}	Time dependent	Carbonated volume	Calculated

V_{carb} is a time-dependent value: the longer is the exposition time to carbonation, the higher is the carbonated volume. The calculation of V_{carb} as a function of time is detailed in the supplementary materials.

Figure 3 shows the final results of CO₂_{uptake} calculation for the OPC_{aer} using Eq (6). After a use phase of 50 years, OPC_{aer} presents a CO₂_{uptake} of 1.66 kg. This value of CO₂_{uptake} is approximately 63% of the maximum value of CO₂ that can be carbonized by the total volume of OPC_{aer} (2.61 kg of CO₂). Therefore, during the end-of-life phase, OPC_{aer} can absorb up to 0.95 kg of CO₂.

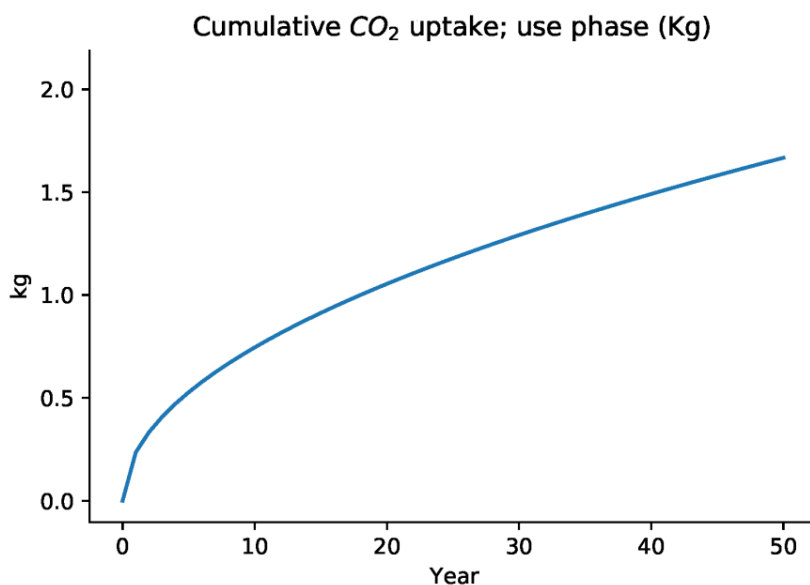


Figure 3. Cumulative CO₂ uptake for the use phase, over 50 years, for the OPC_{aer}.

3.3.2.2. Carbonation rate for alkali-activated aerated SSS and goethite-based inorganic polymers

While carbonation in the atmospheric environment has been extensively studied for OPC-based concrete, the carbonation of alkali-activated materials and inorganic polymers is still controversial and debated in the scientific community. Therefore, there is no universally accepted mathematical or empirical model to assess the carbonation rate of alkali-activated materials and inorganic polymers. A precise determination of the carbonation resistance for alkali-activated materials and inorganic polymers would require an extensive lab and field tests campaign, going beyond the scope of this study. Consequently, the carbonation rate during the use-phase for SSS_{aer} and GIP considered in this study is based on assumptions, leading to some uncertainty of the results, due to the lack of data on carbonation rate for materials other than OPC-based concrete.

As described above, the carbonation of OPC_{aer} occurs mostly due to the reaction of atmospheric CO₂ with the calcium in Ca(OH)₂ present in the binder [67]. In the case of SSS_{aer}, SSS used as a precursor for the alkali activation has a calcium content (60%) similar to that of OPC. Since the carbonation rate depends on the calcium content, it is assumed that the carbonation rate for the SSS_{aer} is similar to the one for OPC_{aer}.

On the other hand, GIP is synthesised from precursors with a low calcium content. Thus, it has a binder structure rich in alkalis and aluminium and lower in Ca/Si [68]. This different chemistry of the precursors leads to differences in the carbonation mechanism and consequently, to different CO₂ uptake rates than those observed in OPC-based concretes [68–70]. On top of that, some studies showed how the carbonation rate highly depends on the mix design of the inorganic polymer. Inorganic polymers made from different precursors and different mix designs may present significantly different resistance to carbonation [14].

The present study assumes a carbonation rate for GIP based on several accelerated carbonation test results found in the literature [14,68,69,71–73]. These studies tested the carbonation rate of inorganic polymers and geopolymers made from different precursors. In general, all authors reported

that resistance of inorganic polymers to carbonation is rather low, leading to a carbonation rate up to four times higher compared to that of OPC-based concretes. However, the results of these tests vary significantly from case to case, and in some cases, inorganic polymers presented a carbonation rate similar or only slightly higher compared to that of OOPC concrete. Although, for the sake of simplicity, the current study assumes a carbonation rate for GIP identical to that of OPC_{aer} and SSS_{aer} . Results analysis must take into account the uncertainty associated with this assumption.

3.3.3. End-of-life phase

When a structure is demolished, resulting rubbles (in this case made of SSS_{aer} , OPC_{aer} , or GIP) can be recycled as aggregates or landfilled.

If rubbles are landfilled, no pre-treatment is required after demolition. In a landfill, CO_2 uptake occurs through the carbonation of the exposed surfaces. If rubbles are recycled, they are usually pre-treated through a crushing process. Crushing breaks concrete into small pieces, significantly increasing the surface available for carbonation. However, most of the volume is already carbonated during the use phase, so that the carbonation rate is lower compared to that in the use phase.

In the current study, according to the present situation in Belgium, it is assumed that 90% of the concrete is recycled after demolition as low-quality aggregates for road surfaces, while the remaining 10% is landfilled. The end-of-life includes processes of landfilling, carbonation of concrete in a landfill, crushing, and carbonation of recycled aggregates.

The method to estimate CO_2 uptake during end-of-life is similar to that described above for the use phase. The final calculation for CO_2 uptake during the end of life is reported in Figure 4. The detailed calculation to estimate the amount of CO_2 uptake is fully reported in the supplementary materials.

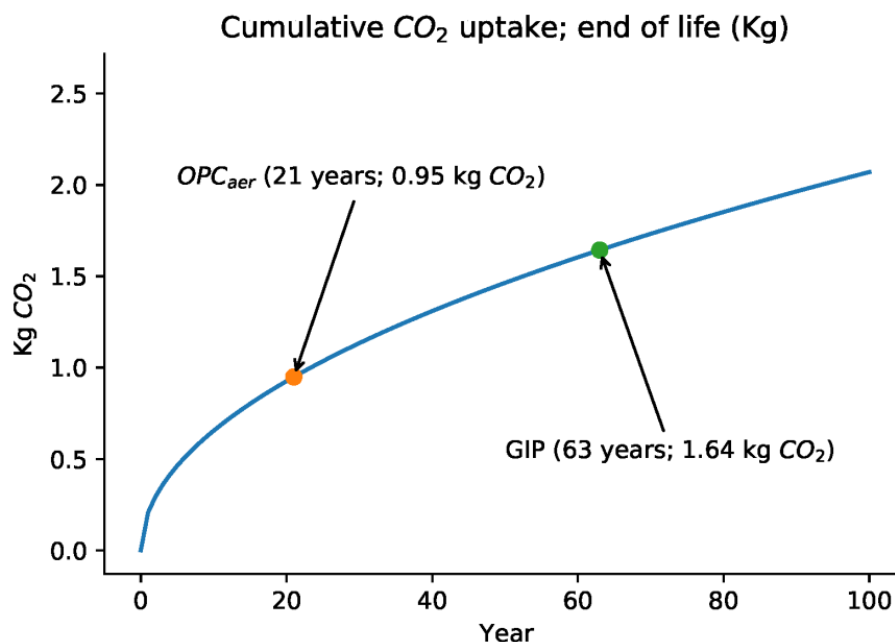


Figure 4. Cumulative CO_2 uptake for the end of life, over 100 years, for OPC_{aer} .

The maximum amount of CO₂ that can be absorbed by the given volume of OPC_{aer} and SSS_{aer} is 2.61 kg. Since 1.66 kg of CO₂ has already been carbonated during the use phase, the maximum amount of CO₂ that can be absorbed during the end of life is equal to 0.95 kg (the point in orange in Figure 4).

Following the assumptions described above, an equal carbonation rate during the end of life is also assumed for GIP. However, the volume of GIP available for carbonation is higher compared to the one calculated for OPC_{aer} and SSS_{aer} (0.063 m³ instead of 0.05 m³, as shown in Table 1). Therefore the maximum amount of CO₂ that can be absorbed is 3.3 kg. Consequently, the CO₂ absorbed at the end of life is 1.64 kg, which is reached after 63 years (point in green in Figure 4), going beyond the declared time horizon.

Therefore, even if the end of life is considered at 100 years following the production of materials, the carbonation effect for OPC_{aer} and SSS_{aer} ends 21 years after the landfilling or recycling of the materials, while it lasts up to 63 years for GIP. The calculated time at which the emissions occur is considered when building the dynamic inventory for the D_GWP, while it cannot be specified when building the inventory for the S_GWP. For the S_GWP, indeed, only the total quantity of CO₂ emitted or uptaken can be specified for each phase (production, use phase, end-of-life). All these emissions are assumed to occur at year zero, and impacts are calculated with a fixed 100 years time horizon. The discrepancy between actual and declared lifetime for static and dynamic inventory, assuming an equal time horizon of 100 years, is shown in Figure 5.

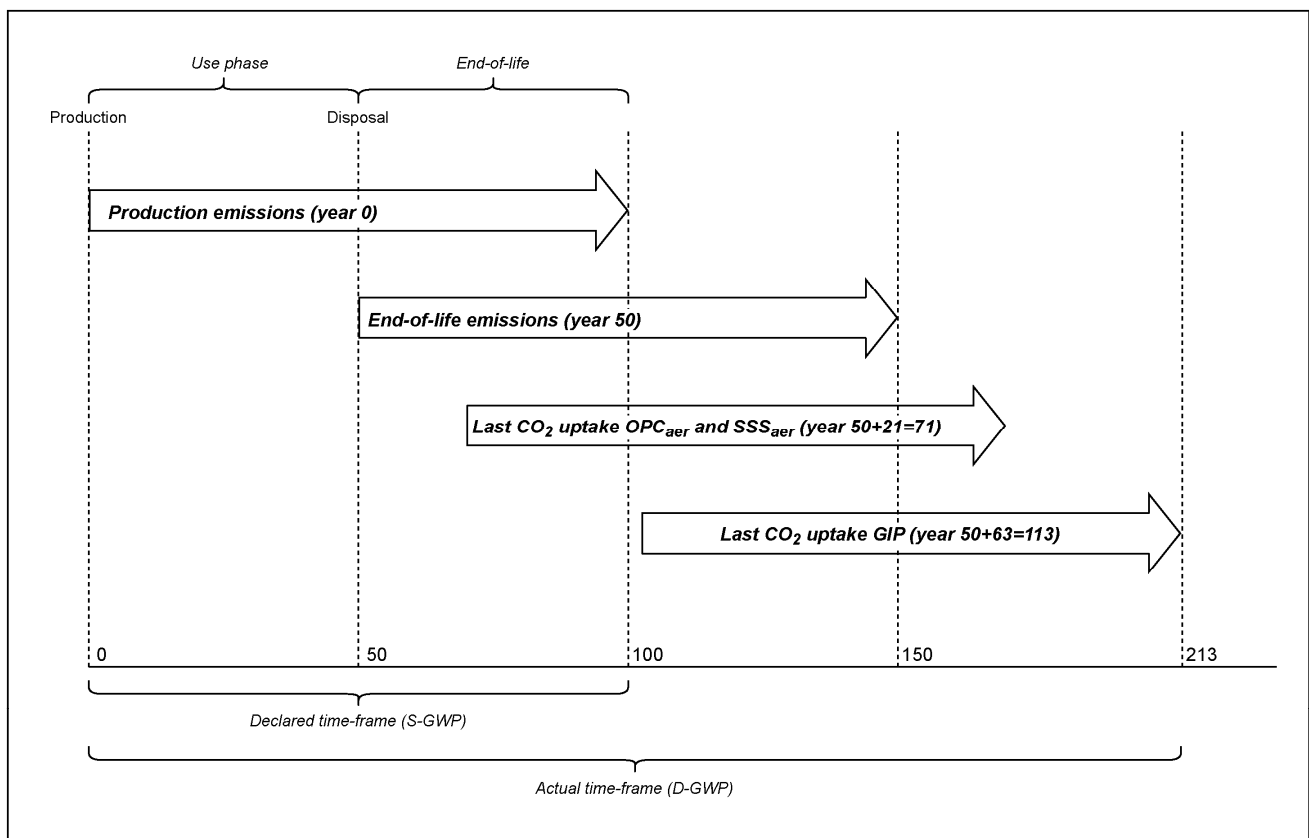


Figure 5. Discrepancies between actual and declared time horizons of the analysis when calculating S_GWP.

4. Results

4.1. Static GWP

Figure 6 reports the S_GWP_{20} and S_GWP_{100} results.

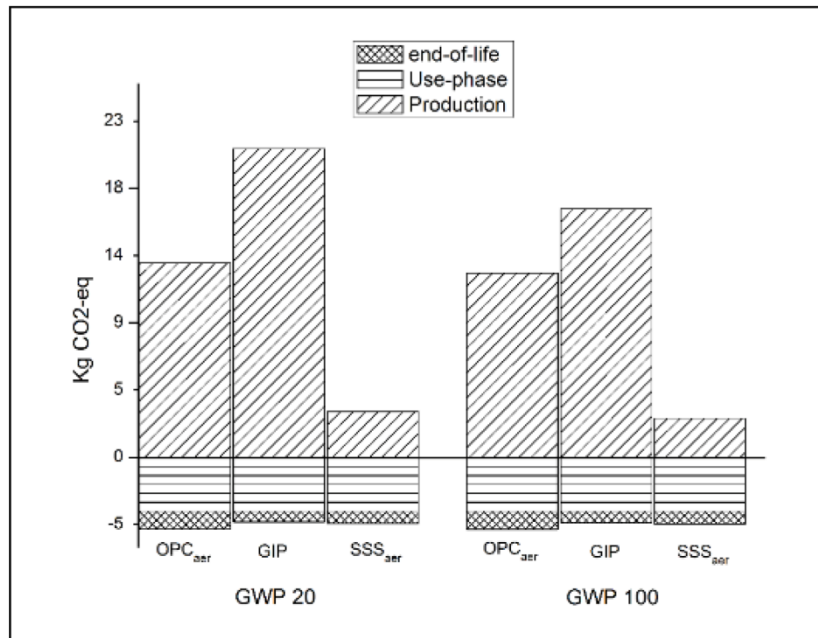


Figure 6. Results for S_GWP (20 and 100 years' time horizon).

For both S_GWP_{20} and S_GWP_{100} , the GIP has the highest global warming impact (37.86 kg CO₂-eq for S_GWP_{20} and 32.9 kg CO₂-eq for S_GWP_{100}), with the highest contribution given by the production phase. OPC_{aer} is the material with the second-highest contribution (10.79 kg CO₂-eq for GWP₂₀ and 10.11 kg CO₂-eq for GWP₁₀₀), while SSS_{aer} is the most favorable option (1.21 kg CO₂-eq for GWP₂₀ and 0.73 kg CO₂-eq for GWP₁₀₀). For all three materials life cycles, most of the impact occurs during the production phase. Carbonation during the use phase is assumed to be equal for the three cases. The impact of the end-of-life phase is negative for the three materials, meaning that the effect of carbonation in the end-of-life is higher than the impact caused by the recycling and transport of the waste material.

Finally, differences in values of GWP₂₀ and GWP₁₀₀ for the production phase of the different materials can be observed. While OPC_{aer} presents very similar values for both time horizons (13 kgCO₂-eq for GWP₂₀ and 12.3 kg CO₂-eq for GWP₁₀₀, corresponding to a 5% decrease), GIP presents a decrease of 13% (40.3 kg CO₂-eq for GWP₂₀ and 35.4 kg CO₂-eq for GWP₁₀₀). This is caused by different amounts of methane for the three materials, as GWP₂₀ is higher than GWP₁₀₀ for short-lived gases. Table 4 shows the kg of emissions for the most relevant GHGs in the production, use and end-of-life phases for the three materials.

Table 4. Most relevant GHGs emissions during the life cycles of the three materials.

	CO ₂ (kg)			CH ₄ (kg)			Other GHGs (kg)		
	OPC _{aer}	GIP	SSS _{aer}	OPC _{aer}	GIP	SSS _{aer}	OPC _{aer}	GIP	SSS _{aer}
Production	12	31	2.3	0.01	0.05	0.007	0.02	0.02	0.002
Use-phase	-1.66	-1.66	-3.6	/	/	/	/	/	/
End-of-life	-0.59	-0.8	-0.26	4·10 ⁻⁴	0.001	9·10 ⁻⁴	1·10 ⁻³	2·10 ⁻³	2·10 ⁻³

Notes: Other GHGs: mostly N₂O and CO.

Most GHG emissions for the production phase of OPC_{aer} are CO₂ (12 kg), with a small emission of methane (0.01 kg). GIP production emits a higher amount of CO₂ (31 kg) but five times more CH₄ than OPC_{aer} (0.05 kg). This higher emission of CH₄ is mostly caused by the electricity consumption in the fuming process and by the long transports.

4.2. Dynamic GWP

Figure 7 shows the instantaneous and cumulative GWI for the three materials. Although the declared time frame of the analysis is 100 years, the results are reported for 213 years, to be consistent with the time frame of the S_{GWP} results.

The graph on the top presents an increase in the instantaneous impact for all materials, due to the emissions occurring during the production. Accordingly, with the results of the S_{GWP}, the GIP presents the highest instantaneous impact in year 1. OPC_{aer} has the second-highest contribution, and SSS_{aer} is the material with the lowest impact. As no other emissions occur during the use phase, between year 1 and year 50, the slope of the three curves is negative, because of the degradation of GHGs in the atmosphere. Moreover, during the use phase, the carbonation process occurs, further increasing the negative slope of the instantaneous curves. Although the carbonation rate is assumed identical for the three materials, GIP presents a steeper curve compared to the curves for OPC_{aer} and SSS_{aer}. As explained in the previous paragraph, this is due to the highest amount of methane emitted during the production of GIP, which is rapidly degraded in the atmosphere.

At year 50, the construction is demolished, and materials are either recycled (90%) or landfilled (10%). The peaks at year 50 are caused by the emissions released during the recycling or landfilling and by transports. In this phase, OPC_{aer} presents a lower pick compared to GIP and SSS_{aer}, due to the lighter weight of OPC_{aer}, which causes lower emissions in the recycling process and transports. From year 50 till year 71 for OPC_{aer} and SSS_{aer}, and year 113 for GIP, the carbonation process continues, decreasing the instantaneous global warming impact of the three materials. The CO₂ uptake in the end-of-life occurs at a lower rate compared to the use phase. Finally, although after year 71 and 113 the carbonation processes stop, the GHGs emitted continues degrading in the atmosphere, and the slope of the three curves remains negative. Considering thousands of years as the time frame of the analysis, the three curves tend towards an equilibrium value. Only in the case of SSS_{aer}, the instantaneous impact can reach again an instantaneous impact equal to zero. In the case of GIP and OPC_{aer}, it will take several thousands of years to reach an instantaneous impact equal to zero again.

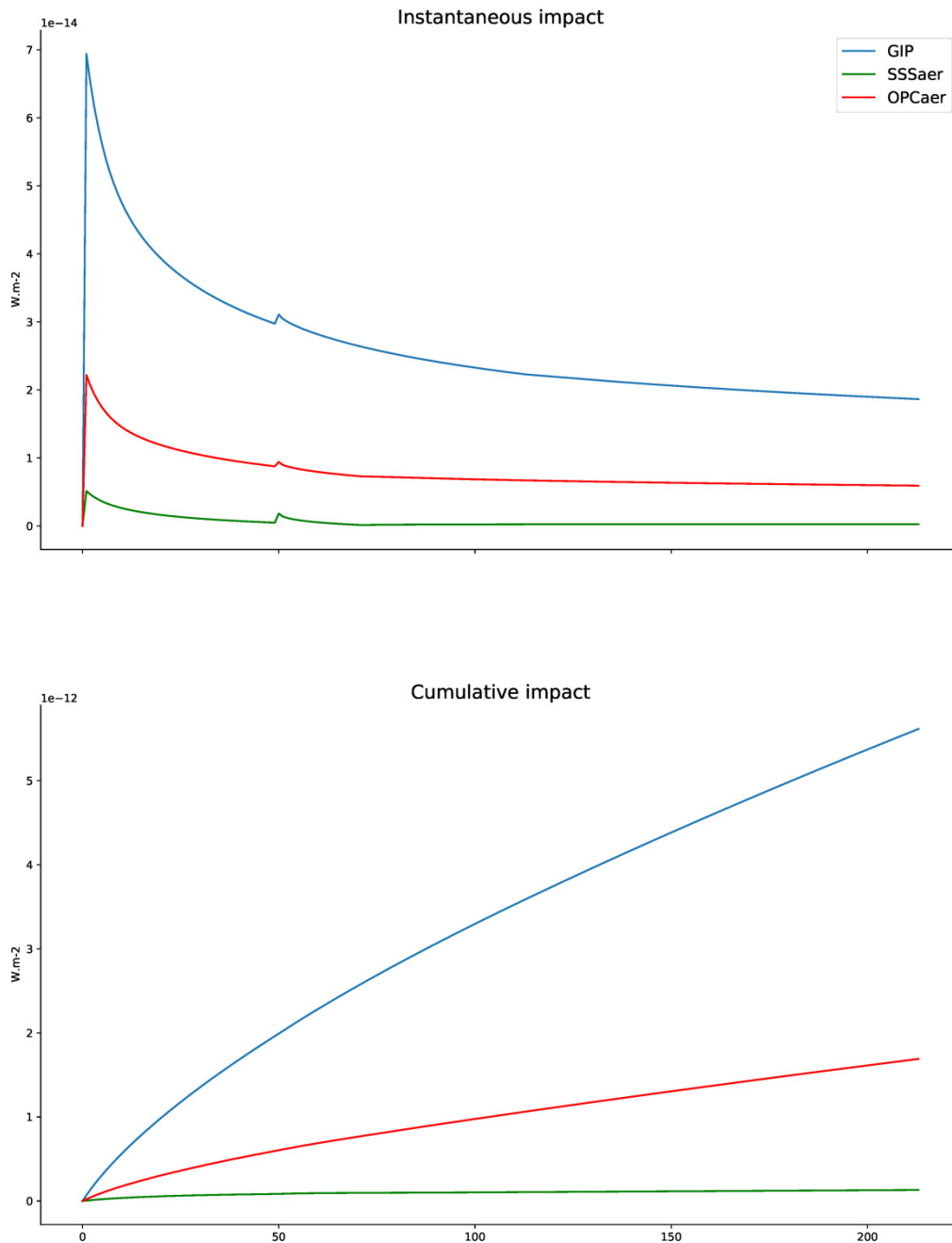


Figure 7. Dynamic GWP results.

As explained before, in the case of the S_GWP , the time horizons chosen for GWP are not consistent with the actual time frame of the study. To quantify this inconsistency, it is interesting to compare the ranking of the three materials, by using the S_GWP (expressed in CO_2 -equivalent) and the cumulative impact for the D_GWP (expressed as W/m^2) for 20- and 100-year time horizons. While in the case of S_GWP all emissions are considered to occur at year zero, the D_GWP allows selecting the exact cumulative impact calculated 20 years after the last emission, which means 91 years (71 years +20 years) for OPCaer and SSSaer, and 133 years for GIP (113 years + 20 years). Similar reasoning can be done for the GWP and cumulative impact calculated 100 years after the last

emission. Table 5 and Figure 8 show the comparison between the static and dynamic approach for 20 and 100 years time horizons. The numbers are expressed as percentages of the impact for GIP, which is the highest impact among the three materials (expressed as 100%).

Although the ranking of the materials does not change, the gap between materials is different depending on the time horizon and on the approach used. In both 20 years and 100 years' time horizons, the dynamic approach gives a lower impact to OPC_{aer} compared to the static.

Significant differences are also found for SSS_{aer}. For the 20 years' time horizons, the static approach gives a negative value (−1.7%), while the dynamic result is positive (2.5%). As indeed shown in the cumulative impact analysis above, the impact for SSS_{aer} always stays positive. In the same manner, at 100 years' time horizons, the static approach overestimates the negative impacts for SSS_{aer}. This may be due to the inconsistency between the calculated time frame of the study (100 years), and the actual time frame (171 years).

Table 5. Comparison of the results obtained with traditional and dynamic approaches for 20 and 100 years' time horizon.

	OPC _{aer}	GIP	SSS _{aer}
20 years time horizon			
Static (%)	28.4	100	−1.7
Dynamic (%)	22.7	100	2.5
	(91 years)	(133 years)	(91 years)
100 years time horizon			
Static (%)	30.6	100	−2.6
Dynamic (%)	25.6	100	2.1
	(171 years)	(213 years)	(171 years)

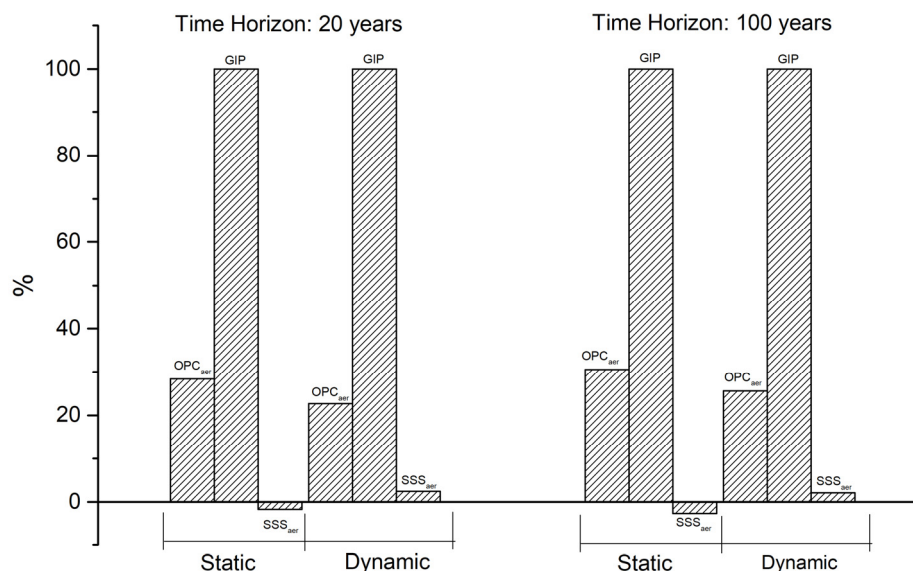


Figure 8. Comparison static vs dynamic for 20 and 100 years time horizons.

4.3. Results interpretation and limitation of the study

The dynamic global warming impact calculation provided similar results than the static approach, although it also generated more detailed information on the global warming impact over time. Firstly, it generated essential variations while comparing the different scenarios. Secondly, it allows having a more informed analysis of the emissions flows and on the trend of the radiative forcing curves, overcoming the time-related inconsistencies found in the static approach.

The results described above show that for any time horizon, the GIP is the material presenting the highest global warming impacts, both for the static and the dynamic approach. OPC_{aer} presents the second highest, while SSS_{aer} has the lowest impact. During the use phase and the end-of-life phase, the carbonation process can partially reabsorb the CO₂ emitted during the production phase, lowering the final impact of the materials. The study assumes an equal carbonation rate for all three materials. However, according to the mathematical model used in the study, the carbonation can uptake a maximum of 2.61 kg of CO₂. This uptake has a limited effect if compared to the CO₂ emissions caused by the production of GIP (31 kg CO₂) and OPC_{aer} (12 kg). The carbonation effect becomes more significant for the SSS_{aer}, because of the lower CO₂ emissions in the production phase (2.3 kg). The assumption of an equal carbonation rate for all materials brings however high uncertainty to the final results. Several lab-test results indicated potential carbonation for industrial slag-based material up to four times higher than OPC-based concretes. However, a general rule cannot be drawn, as the carbonation rate is specific for each material. A more specific lab and field tests campaign is therefore strongly advised to study the carbonation process for SSS_{aer} and GIP deeply. On the other hand, it is important to underline that higher carbonation can affect the resistance of the steel bars if the material is used in reinforced concrete. Therefore, the balance between environmental benefits and technical risks should be always considered.

5. Conclusions

This study compares static and dynamic approaches to calculate and compare the global warming impact during the life cycle of three different lightweight construction blocks: (i) a traditional autoclaved aerated OPC-based concrete (OPCaer); (ii) a goethite-based inorganic polymer (GIP); (iii) an alkali-activated aerated SSS block (SSSaer) based on stainless steel slag.

For any time horizon, GIP is the material with the highest impact, using both static and dynamic approaches, due to the high energy consumption in the process of goethite fuming. OPC_{aer} has the second-highest global warming impact, while SSS_{aer} is the material with the lowest global warming impact. Dynamic GWP (D_GWP) has shown more consistency when stating the actual time frame of the study. A D_GWP allows indeed a more informed analysis of emission flows and radiative forcing effect over time, leading to a more accurate analysis of long-term effects of global warming. Therefore, D_GWP can potentially help decision-makers to improve their understanding of when potential impacts may occur and, consequently, provide more informed decision support.

However, it is important to notice that the consideration of future emissions required to build a dynamic inventory may lead to high uncertainty of the results. For instance, the carbonation rate considered in the study for GIP and SSS_{aer} is assumed to be equal to the one calculated for OPC_{aer}. This assumption leads to high uncertainty of the results. Although further research on the carbonation process is strongly needed, the study proved how the dynamic approach in GWP provides more

detailed information on when an impact occurs, and on the resilience time needed by the atmosphere to regain the initial status.

Acknowledgments

The authors are grateful to the Research Foundation – Flanders (FWO) for their financial support, making possible the collaboration between KU Leuven and the Polytechnique Montréal.

Conflict of interest

No conflict of interest is declared by the authors.

References

1. Kylili A, Fokaides PA (2017) Policy trends for the sustainability assessment of construction materials: A review. *Sustain Cities Soc* 35: 280–288.
2. Häfliger IF, John V, Passer A, et al. (2017) Buildings environmental impacts' sensitivity related to LCA modelling choices of construction materials. *J Clean Prod* 156: 805–816.
3. Pontikes Y, Snellings R (2014) Chapter 16 - Cementitious Binders Incorporating Residues, Boston, Elsevier, 219–229.
4. Panesar DK (2019) Supplementary cementing materials, *Developments in the Formulation and Reinforcement of Concrete*, Elsevier, 55–85.
5. Di Filippo J, Karpman J, DeShazo JR (2019) The impacts of policies to reduce CO₂ emissions within the concrete supply chain. *Cem Concr Compos* 101: 67–82.
6. Myhre G, Shindell D, Bréon FM, et al. (2013) Anthropogenic and Natural Radiative Forcing, In: Stocker TF, Qin D, Plattner G-K, et al. (Eds.), *Climate Change 2013: The Physical Science Basis. Contribution of Working Group I to the Fifth Assessment Report of the Intergovernmental Panel on Climate Change*, Cambridge, UK, Cambridge University Press, 659–740.
7. Allen MR, Shine KP, Fuglestedt JS, et al. (2018) A solution to the misrepresentations of CO₂-equivalent emissions of short-lived climate pollutants under ambitious mitigation. *Npj Clim Atmos Sci* 1: 16.
8. Dyckhoff H, Kasah T (2014) Time Horizon and Dominance in Dynamic Life Cycle Assessment. *J Ind Ecol* 18: 799–808.
9. Pigné Y, Navarrete Gutiérrez T, Gibon T, et al. (2020) LCI METHODOLOGY AND DATABASES A tool to operationalize dynamic LCA, including time differentiation on the complete background database. *Int J Life Cycle Assess* 25: 267–279.
10. Reap J, Roman F, Duncan S, et al. (2008) A survey of unresolved problems in life cycle assessment. *Int J Life Cycle Assess* 13: 374.
11. Shimako AH, Tiruta-Barna L, Bisinella de Faria AB, et al. (2018) Sensitivity analysis of temporal parameters in a dynamic LCA framework. *Sci Total Environ* 624: 1250–1262.
12. Levasseur A, Lesage P, Margni M, et al. (2010) Considering Time in LCA: Dynamic LCA and Its Application to Global Warming Impact Assessments. *Environ Sci Technol* 44: 3169–3174.
13. Levasseur A, Lesage P, Margni M, et al. (2013) Biogenic Carbon and Temporary Storage Addressed with Dynamic Life Cycle Assessment. *J Ind Ecol* 17: 117–128.

14. Pasupathy K, Berndt M, Castel A, et al. (2016) Carbonation of a blended slag-fly ash geopolymer concrete in field conditions after 8 years. *Constr Build Mater* 125: 661–669.
15. Collinge WO, Landis AE, Jones AK, et al. (2013) Dynamic life cycle assessment: framework and application to an institutional building. *Int J Life Cycle Assess* 18: 538–552.
16. Su S, Li X, Zhu Y, et al. (2017) Dynamic LCA Framework for Environmental Impact Assessment of Buildings. *Energy Build* 149: 310–320.
17. Hu M (2018) Dynamic life cycle assessment integrating value choice and temporal factors—A case study of an elementary school. *Energy Build* 158: 1087–1096.
18. Negishi K, Lebert A, Almeida D, et al. (2019) Evaluating climate change pathways through a building's lifecycle based on Dynamic Life Cycle Assessment. *Build Environ* 164: 106377.
19. Resch E, Andresen I, Cherubini F, et al. (2021) Estimating dynamic climate change effects of material use in buildings—Timing, uncertainty, and emission sources. *Build Environ* 187: 107399.
20. Mastrucci A, Marvuglia A, Benetto E, et al. (2020) A spatio-temporal life cycle assessment framework for building renovation scenarios at the urban scale. *Renew Sustain Energy Rev* 126: 109834.
21. Fouquet M, Levasseur A, Margni M, et al. (2015) Methodological challenges and developments in LCA of low energy buildings: Application to biogenic carbon and global warming assessment. *Build Environ* 90: 51–59.
22. Tiruta-Barna L, Pigné Y, Navarrete Gutiérrez T, et al. (2016) Framework and computational tool for the consideration of time dependency in Life Cycle Inventory: proof of concept. *J Clean Prod* 116: 198–206.
23. Fouquet M, Levasseur A, Margni M, et al. (2015) Methodological challenges and developments in LCA of low energy buildings: Application to biogenic carbon and global warming assessment. *Build Environ* 90: 51–59.
24. Su S, Zhang H, Zuo J, et al. (2021) Assessment models and dynamic variables for dynamic life cycle assessment of buildings: a review. *Environ Sci Pollut Res* 28: 26199–26214.
25. Beloin-Saint-Pierre D, Albers A, Hélias A, et al. (2020) Addressing temporal considerations in life cycle assessment. *Sci Total Environ* 743: 140700.
26. IPCC (2014) AR5 Climate Change 2014: Mitigation of Climate Change — IPCC, 2014. Available from: <https://www.ipcc.ch/report/ar5/wg3/>.
27. Shine KP (2009) The global warming potential—the need for an interdisciplinary retrieval. *Clim Change* 96: 467–472.
28. IPCC (2013) Climate Change 2013 The Physical Science Basis Working Group I Contribution To The Fifth Assessment Report of The Intergovernmental Panel On Climate Change Wg I In T Ergov Ernmenta L Pa Nel On climate change, United Kingdom and New York, NY, USA.
29. Ismael MR, Carvalho JM (2003) Iron recovery from sulphate leach liquors in zinc hydrometallurgy. *Miner Eng* 16: 31–39.
30. Yue T, Xu Z, Hu Y, et al. (2018) Magnetic Separation and Recycling of Goethite and Calcium Sulfate in Zinc Hydrometallurgy in the Presence of Maghemite Fine Particles. *ACS Sustainable Chem Eng* 6: 1532–1538.
31. Di Maria A, Van Acker K (2018) Turning Industrial Residues into Resources: An Environmental Impact Assessment of Goethite Valorization. *Engineering* 4: 421–429.
32. Yue T, Niu Z, Tao H, et al. (2019) Green Recycling of Goethite and Gypsum Residues in

- Hydrometallurgy with α -Fe₃O₄ and γ -Fe₂O₃ Nanoparticles: Application, Characterization, and DFT Calculation. *ACS Sustainable Chem Eng* 7: 6821–6829.
33. Van Roosendael S, Roosen J, Banerjee D, et al. (2019) Selective recovery of germanium from iron-rich solutions using a supported ionic liquid phase (SILP). *Sep Purif Technol* 221: 83–92.
 34. Szewczuk-Karpisz K, Krasucka P, Boguta P, et al. (2019) Anionic polyacrylamide efficiency in goethite removal from aqueous solutions: goethite suspension destabilization by PAM. *Int J Environ Sci Technol* 16: 3145–3154.
 35. Van Roosendael S, Regadío M, Roosen J, et al. (2019) Selective recovery of indium from iron-rich solutions using an Aliquat 336 iodide supported ionic liquid phase (SILP). *Sep Purif Technol* 212: 843–853.
 36. Rodriguez Rodriguez N, Onghena B, Binnemans K (2019) Recovery of Lead and Silver from Zinc Leaching Residue Using Methanesulfonic Acid. *ACS Sustainable Chem Eng* 7: 19807–19815.
 37. Rodriguez Rodriguez N, Machiels L, Onghena B, et al. (2020) Selective recovery of zinc from goethite residue in the zinc industry using deep-eutectic solvents. *RSC Adv* 10: 7328–7335.
 38. Abo Atia T, Spooren J (2020) Microwave assisted alkaline roasting-water leaching for the valorisation of goethite sludge from zinc refining process. *Hydrometallurgy* 191: 105235.
 39. Wang Z, Liu Y, Qu Z, et al. (2021) In situ conversion of goethite to erdite nanorods to improve the performance of doxycycline hydrochloride adsorption. *Colloids Surfaces A Physicochem Eng Asp* 614: 126132.
 40. Huda N, Naser J, Brooks G, et al. (2012) Computational Fluid Dynamic Modeling of Zinc Slag Fuming Process in Top-Submerged Lance Smelting Furnace. *Metall Mater Trans B* 43: 39–55.
 41. Nagraj S, Chintinne M, Guo M, et al. (2020) A Dynamic Model of a Submerged Plasma Slag Fuming Process, In: *Minerals, Metals and Materials Series*, Springer, 237–245.
 42. Verscheure K, Van Camp M, Blanpain B, et al. (2007) Continuous Fuming of Zinc-Bearing Residues: Part I. Model Development. *Metall Mater Trans B* 38: 13–20.
 43. Verscheure K, Camp M Van, Blanpain B, et al. (2007) Continuous Fuming of Zinc-Bearing Residues: Part II. The Submerged-Plasma Zinc-Fuming Process. *Metall Mater Trans B* 38: 21–33.
 44. Alemán JV, Chadwick AV, He J, et al. (2009) Definitions of terms relating to the structure and processing of sols, gels, networks, and inorganic-organic hybrid materials (IUPAC Recommendations 2007). *Pure Appl Chem* 79: 1801.
 45. van Deventer JSJ, Provis JL, Duxson P, et al. (2010) Chemical Research and Climate Change as Drivers in the Commercial Adoption of Alkali Activated Materials. *Waste Biomass Valorization* 1: 145–155.
 46. Sofilić T, Rastovčan-Mioč A, Cerjan-Stefanović Š, et al. (2004) Characterization of steel mill electric-arc furnace dust. *J Hazard Mater* 109: 59–70.
 47. Rosales J, Agrela F, Entrenas JA, et al. (2020) Potential of stainless steel slag waste in manufacturing self-compacting concrete. *Materials (Basel)* 13.
 48. Wang X, Geysen D, Van Gerven T, et al. (2017) Characterization of landfilled stainless steel slags in view of metal recovery. *Front Chem Sci Eng* 11: 353–362.
 49. Adamczyk B, Brenneis R, Adam C, et al. (2010) Recovery of Chromium from AOD-Converter Slags. *Steel Res Int* 81: 1078–1083.
 50. Durinck D, Engström F, Arnout S, et al. (2008) Hot stage processing of metallurgical slags.

- Resour Conserv Recycl* 52: 1121–1131.
51. Durinck D, Arnout S, Mertens G, et al. (2008) Borate Distribution in Stabilized Stainless-Steel Slag. *J Am Ceram Soc* 91: 548–554.
 52. Salman M, Cizer Ö, Pontikes Y, et al. (2014) Effect of accelerated carbonation on AOD stainless steel slag for its valorisation as a CO₂-sequestering construction material. *Chem Eng J* 246: 39–52.
 53. Salman M, Dubois M, Di Maria A, et al. (2016) Construction Materials from Stainless Steel Slags: Technical Aspects, Environmental Benefits, and Economic Opportunities. *J Ind Ecol* 20: 854–866.
 54. Di Maria A, Salman M, Dubois M, et al. (2018) Life cycle assessment to evaluate the environmental performance of new construction material from stainless steel slag. *Int J Life Cycle Assess* 1–19.
 55. Iacobescu RI, Angelopoulos GN, Jones PT, et al. (2016) Ladle metallurgy stainless steel slag as a raw material in Ordinary Portland Cement production: a possibility for industrial symbiosis. *J Clean Prod* 112: 872–881.
 56. Provis J, van Deventer J (2014) Alkali Activated Materials - State-of-the-Art Report, RILEM TC, John Provis, Springer.
 57. Pommer K, Pade C (2006) Guidelines -uptake of carbon dioxide in the life cycle inventory of concrete, Oslo, Norway, Dansk Teknologisk Institut, Nordic Innovation Centre.
 58. European Commission (2015) Screening template for Construction and Demolition Waste management in Belgium.
 59. Di Maria A, Eyckmans J, Van Acker K (2018) Downcycling versus recycling of construction and demolition waste: Combining LCA and LCC to support sustainable policy making. *Waste Manag* 75: 3–21.
 60. Martaud T (2008) Evaluation environnementale de la production de granulats en exploitation de carrières. Indicateurs, Modèles et Outils, Géologie appliquée, Université d'Orléans.
 61. Mroueh U-M, Eskola P, Laine-Ylijoki J, et al. (2000) Life cycle assessment of road construction, Helsinki, Finland.
 62. Dewar J (2003) Concrete mix design, In: Newman JB, Choo BS (Eds.), *Advanced concrete technology*, Oxford, Butterworth-Heinemann, 3–40.
 63. Kjellsen KO, Guimaraes M, Nilsson A (2005) The CO₂ Balance of Concrete in a Life Cycle Perspective, Oslo, Norway.
 64. Lagerblad B (2006) CO₂ uptake during concrete life cycle- state of the art, Oslo, Norway.
 65. Pommer K, Pade C (2006) Guidelines -uptake of carbon dioxide in the life cycle inventory of concrete, Oslo, Norway.
 66. Kelleberg D, Althaus HJ, Kunniger T, et al. (2007) Life Cycle Inventories of Building Products. Ecoinvent report No. 7, Dübendorf.
 67. Castellote M, Fernandez L, Andrade C, et al. (2009) Chemical changes and phase analysis of OPC pastes carbonated at different CO₂ concentrations. *Mater Struct* 42: 515–525.
 68. Van Deventer JSJ, Provis JL, Duxson P (2012) Technical and commercial progress in the adoption of geopolymers. *Miner Eng* 29: 89–104.
 69. Bernal SA, Provis JL, Brice DG, et al. (2012) Accelerated carbonation testing of alkali-activated binders significantly underestimates service life: The role of pore solution chemistry. *Cem Concr Res* 42: 1317–1326.

70. Gruskovnjak A, Lothenbach B, Holzer L, et al. (2006) Hydration of alkali-activated slag: comparison with ordinary Portland cement. *Adv Cem Res* 18: 119–128.
71. Adam A (2009) Strength and durability properties of alkali activated slag and fly ash-based geopolymer concrete, Australia, RMIT University Melbourne.
72. Bakharev T, Sanjayan JG, Cheng YB (2001) Resistance of alkali-activated slag concrete to carbonation. *Cem Concr Res* 31: 1277–1283.
73. Ul Haq E, Padmanabhan SK, Licciulli A (2014) In-situ carbonation of alkali activated fly ash geopolymer. *Constr Build Mater* 66: 781–786.



AIMS Press

© 2021 the Author(s), licensee AIMS Press. This is an open access article distributed under the terms of the Creative Commons Attribution License (<http://creativecommons.org/licenses/by/4.0>)